

Magnetic dichroism in angular resolved hard X-ray photoelectron spectroscopy from buried magnetic layers.

Carlos E. ViolBarbosa, Siham Ouardi, Gerhard H. Fecher*, Daniel Ebke,
Claudia Felser

*Max Planck Institute for Chemical Physics of Solids, Nöthnitzer Str. 40, 01187 Dresden,
Germany*

Abstract

This work reports on the measurement of magnetic dichroism in angular-resolved photoelectron spectroscopy from in-plane magnetized buried thin films. The high bulk sensitivity of hard X-ray photoelectron spectroscopy (HAXPES) in combination with circularly polarized radiation enables the investigation of the magnetic properties of buried layers. Angular distributions of high kinetic energy (7 to 8 keV) photoelectrons in a range of about 60° were recorded in parallel to the energy distribution. Depending on purpose, energy and angular resolutions of 150 to 250 meV and 0.17° to 2° can be accomplished simultaneously in such experiments. Experiments were performed on exchange-biased magnetic layers covered by thin oxide films. More specifically, the angular distribution of photoelectrons from the ferromagnetic layer Co_2FeAl layer grown on MnIr exchange-biasing layer was investigated where the magnetic structure is buried beneath a MgO layer. Pronounced magnetic dichroism is found in the Co and Fe $2p$ states for all angles of emission. A slightly increased magnetic dichroism was observed for normal emission in agreement with theoretical considerations.

Keywords: Hard X-ray photoelectron spectroscopy, HAXPES, Circular magnetic dichroism, Angular resolved photoelectron spectroscopy

*Corresponding author: Gerhard H. Fecher, fecher@cpfs.mpg.de

1. Introduction

Magnetic circular dichroism (MCD) in photoabsorption and photoemission has become a very powerful tool for the element-specific investigation of the magnetic properties of alloys and compounds. Thus far, such studies have been mainly carried out using soft X-rays, resulting in a rather surface sensitive technique due to the low electron mean free path of the resulting low energy electrons. The application of hard X-rays [1] results in the emission of electrons with high kinetic energies allowing an increase of probing depth [2]. For $h\nu > 8$ keV, the bulk spectral weight was found to reach more than 95% [3]. Hard X-ray photoelectron spectroscopy (HAXPES) has been found to be a well-adaptable non-destructive technique for the analysis of chemical and electronic states [4, 5]. It was recently shown that HAXPES can be combined easily with variable photon polarization when using phase retarders [6]. Linear dichroism in the angular distribution of the photoelectrons is achieved using linearly polarized hard X-rays and is successfully applied to identify the symmetry of valence band states in Heusler compounds [7]. In combination with excitation by circularly polarized X-rays [6], this method will serve as a unique tool for the investigation of magnetoelectronic properties of deeply buried layers and interfaces in magnetic multilayer structures.

Baumgarten *et al* [8] carried out a pioneering study on magnetic dichroism in photoemission and observed this phenomenon in the core-level spectra of transition metals. The effect, however, was rather small (few %) because of the limited resolution of the experiment. It was later shown that dichroic effects are also obtained using linearly or even unpolarized photons [9, 10]. The observed intensity differences in photoemission are essentially a phenomenon specific to angular-resolved measurements, and therefore, these have been termed as magnetic circular dichroism in the angular distribution (MCDAD) [11, 12, 13]. Recently, Kozina *et al* [14] reported strong dichroism in the HAXPES of ferromagnetic CoFe and Co₂FeAl films in exchange bias structure using MnIr, these being typical materials used in tunnel magnetoresistive devices. Noteworthy, even the Co 3p peak, which is overlapped by the Ir 4f peak, could be identified by this technique thanks to the magnetic dichroism effect in that energy position. [14] These results have proved the reliability and power of HAXPES in the study of magnetic properties in buried layers.

This report presents a study of the angular and energy dependence of the magnetic dichroism in photoemission using hard X-ray excitation. The

dichroism of exchange-biased structures with epitaxially grown ferromagnetic layers of CoFe and Co₂FeAl is investigated. For this purpose the recently installed wide-angle lens system of the HAXPES end-station of beamline BL47XU of Spring-8 (Japan) was used. The lens system has the ability to correct spherical aberrations over wide aperture angles, strongly enhancing the acceptance angle of the high-energy VG Scienta R4000-HV hemispherical analyzer from about 12° to about 60°. [15, 16]

2. Theory of magnetic circular dichroism in the angular distribution of photoelectrons: MCDAD

Theoretical atomic single-particle models were quite successful in describing, explaining, and predicting many aspects of magnetic dichroism. Cherepov *et al* [11] elaborated the general formalism for the dichroism in photoemission excited by circularly, linearly, and unpolarized radiation. They showed that MCDAD is very sensitive to the geometry of the experiment and depends strongly on the relative orientation between the magnetization, helicity, and momentum of the excited electrons. The maximum effect is obtained when the magnetization and helicity vectors are parallel; the effect decreases with an increase in the angle between these vectors. The electronic states in solids usually do not carry a spherical or axial symmetry as in free atoms but have to follow the symmetry of the crystal [17]. The angular distribution $I^j(\mathbf{k}, \mathbf{n})$ of the photoemitted electrons – as derived for example in Reference [11] for the case of axially symmetric polarized atoms – has to account for the non-diagonal density matrix $\rho_{NM'_N}^{\mathbf{n}}$ [18]. This leads to the following equation for the case of a non-axial symmetry:

$$I^j(\mathbf{k}, \mathbf{n}) = \frac{c_\sigma}{[l]} \sqrt{\frac{3[j]}{4\pi}} \sum_{\kappa, L} \sum_N [N]^{1/2} C_{\kappa LN}^j \times \sum_{x, M} \sum_{M_N, M'_N} \rho_{\kappa x}^\gamma \rho_{NM'_N}^{\mathbf{n}}(j) Y_{LM}^*(\mathbf{k}) D_{M_N M'_N}^N(\Omega) \begin{pmatrix} \kappa & L & N \\ x & M & M_N \end{pmatrix}$$

l and j are the orbital and the total angular momentum of an electron in the initial state. $C_{\kappa LN}^j$ are the dynamic parameters derived from the radial matrix elements and $\rho_{\kappa x}^\gamma$ are photon state multipoles [18]. $D_{mm_j}^j(\Omega)$ is the Wigner rotation matrix with Ω being the set of Euler angles describing the rotation from the laboratory to the atomic coordinate frame. The direction

of the electron momentum $\vec{k} = \mathbf{k}(\theta, \phi)$ is defined by the angles θ and ϕ (see Figure 1). Finally, c_σ is a photon-energy ($h\nu$) dependent constant: $c_\sigma = \frac{4\pi^2\alpha}{3} h\nu$ where α is the fine structure constant.

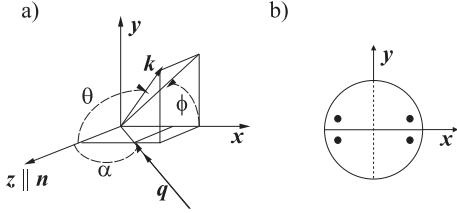


Figure 1: (a) The coordinate system used for the investigation of photoemission. $\mathbf{k}(\theta, \phi)$ is the electron momentum, q is the photon beam and n is the principal axis of alignment. θ and ϕ are the angles defining the direction of the outgoing photoelectrons. α is the angle of photon incidence (in the XZ plane) as defined in optics. It is seen that the angle describing the photon propagation in spherical coordinates is given by $\Theta_q = \alpha + \pi$. The direction of the z axis corresponds to the quantization axis \mathbf{n} . (b) The direction of the in-plane axes x and y is illustrated for an object with C_{2v} symmetry.

This formalism can also be used to consider open shell atoms and the multiplets resulting from the interaction between the core states and the open shell valence states. In that case, the dynamic parameters $C_{J\kappa LN}^j$ have to be calculated for the appropriate coupling scheme (jj , LSJ, or intermediate) with the single particle quantum numbers j, m being replaced by those (J, M) describing the complete atomic state [11]. In that case, the dynamic parameter will redistribute the single-electron results in a particular way over the states of a multiplet (see References [19, 20, 21, 22, 23]).

The state multipoles of the s and p states that define the intensity and the sign and magnitude of the dichroism are summarized in Table 1. Note that the state multipoles are independent of the orbital angular momentum L , they depend only on the total angular momentum J and its projection M_J .

Table 1: State multipoles of $|L, J\rangle = |0, 1/2\rangle, |1, 1/2\rangle, |1, 3/2\rangle$, and $|2, 3/2\rangle$ states.

J M_J	$\frac{1}{2}$ $+\frac{1}{2}$	$-\frac{1}{2}$	$\frac{3}{2}$ $+\frac{3}{2}$	$+\frac{1}{2}$	$-\frac{1}{2}$	$-\frac{3}{2}$
ρ_{00}	$\frac{1}{\sqrt{2}}$	$\frac{1}{\sqrt{2}}$	$\frac{1}{2}$	$\frac{1}{2}$	$\frac{1}{2}$	$\frac{1}{2}$
ρ_{10}	$\frac{1}{\sqrt{2}}$	$-\frac{1}{\sqrt{2}}$	$\frac{3}{2\sqrt{5}}$	$\frac{1}{2\sqrt{5}}$	$-\frac{1}{2\sqrt{5}}$	$-\frac{3}{2\sqrt{5}}$
ρ_{20}	-	-	$\frac{1}{2}$	$-\frac{1}{2}$	$-\frac{1}{2}$	$\frac{1}{2}$
ρ_{30}	-	-	$\frac{1}{2\sqrt{5}}$	$-\frac{3}{2\sqrt{5}}$	$\frac{3}{2\sqrt{5}}$	$-\frac{1}{2\sqrt{5}}$

2.1. Equations for grazing incidence geometry.

In the following, let us consider the special case of geometry of the experiments as described below. A small deviation caused by the finite angle (1°) of the X-rays with respect to the surface will be neglected. The photons are impinging in the $x - z$ plane with unit vector of the photon momentum $\hat{q} = (-\cos(\alpha), -\sin(\alpha), 0)$. At such a grazing incidence with $\alpha = \pi/2$ it becomes $\hat{q} = (-1, 0, 0)$. The electrons are observed in the direction perpendicular to the photon beam ($\theta = \frac{\pi}{2} - \alpha$) with the momentum $\hat{k} = (-\sin(\theta), 0, \cos(\theta))$. At a photon incidence of $\alpha = \pi/2$ and normal emission it becomes $\hat{k} = (0, 0, 1)$. (Compare also Figures 1 and 2.)

Now examine the case: $\vec{n} \rightarrow -\vec{n}$ where the magnetic dichroism emerges from a switching of the direction of magnetization with the initial direction $\vec{n} = (1, 0, 0)$ that is along the x -axis. Applying Equation (2) and the state multipoles of Table 1 the circular magnetic dichroism in the experimental geometry is given for p -states ($J = 1/2, 3/2$) by the simple equation:

$$MCDAD^{\sigma\pm}(p_J) = \mp \rho_{10} \left(\sqrt{\frac{1}{3}} C_{JkLN}^{(1,0,1)} - \sqrt{\frac{1}{15}} C_{JkLN}^{(1,2,1)} + \sqrt{\frac{3}{10}} C_{JkLN}^{(1,2,1)} \cos^2(\theta) \right) \quad (1)$$

The magnetic circular dichroism in the angular distribution (MCDAD) for opposite helicity of the photons has an opposite sign. The equations for the $p_{1/2}$ and $p_{3/2}$ states are the same. The magnitude differs, however, because of the differences in the state multipoles ρ_{10} and dynamical parameters C_{JkLN} . The \cos^2 function in Equation (1) leads to a rather smooth variation of the magnetic dichroism in the geometry used for the present experiment.

3. Experimental details

DC/RF magnetron sputtering was used for the preparation of half of the stack for magnetic tunnel junctions. All films were deposited at room temperature. The argon process pressure was set to 1.5×10^{-3} mbar in the sputtering system where the base pressure was about 10^{-7} mbar. The layers were deposited on thermally oxidized SiO_2 substrates in the following order:

- i) Ta(5) / Ru(30) / MnIr(10) / CoFe(10) / MgO(2)
- ii) Ta(5) / Ru(30) / MnIr(10) / Co_2FeAl (10) / MgO(2)

The numbers in brackets give the corresponding layer thickness in nm. The stack sequence is sketched in Figure 2a. The samples were annealed at 275°C for 10 min in vacuum (5×10^{-2} Pa) in a magnetic field of 0.1 T to provide exchange biasing of the ferromagnetic layer through the MnIr/CoFe(Co_2FeAl) interface (see also [24]), in such a way the CoFe or Co_2FeAl layers are kept magnetized in preset directions.

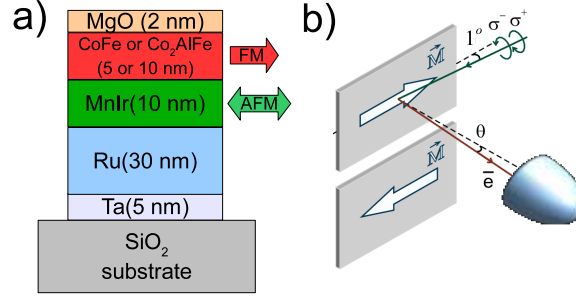


Figure 2: (Color online) (a) Sketch of the exchange-biased films used in the dichroism experiments.

(b) Scheme of the experimental geometry. The incidence angle of the circularly polarized photons was fixed to 1° . X-rays of opposite helicity (σ^+ and σ^-) were provided by a phase retarder. Identical samples with opposite directions of magnetization are used to avoid the necessity of magnetization reversal by external high magnetic fields. The in-plane magnetization M is nearly parallel to the beam axis in order to maximize the dichroism. The photoelectrons are detected over a large range of emission angles θ .

The HAXPES experiments with an excitation energy of 7.940 keV were performed at beamline BL47-XU of SPring-8 [25]. The energy and angular distribution of the photoexcited electrons was analyzed using a high energy VG Scienta R4000-HV hemispherical analyzer, in front of which a wide-acceptance objective lens [15, 16] was placed. The effective acceptance angle

was enlarged to about 60° with an angular resolution of 1° . The overall energy resolution was about 250 meV depending on pass energy and setting of the monochromator. The angle between the electron spectrometer and the photon propagation was fixed at 90° . The impinging angle was set to 1° (resulting in $\theta = -89^\circ$) in order to ensure that the polarization vector of the circularly polarized photons is nearly parallel (σ^-) or antiparallel (σ^+) to the in-plane magnetization M^+ (see Fig 1b). The sign of the magnetization was varied by mounting identical samples with opposite directions of magnetization (M^+ , M^-). This allowed to probe the dichroism by varying both the direction of magnetization and the direction of helicity. The vertical spot size on the sample is $30\text{ }\mu\text{m}$, while in horizontal direction, along the entrance slit of the analyzer, the spot was stretched to approximately 7 mm. The polarization of the incident photons was varied using an in-vacuum phase retarder based on a $600\text{-}\mu\text{m}$ -thick diamond crystal with (220) orientation [26]. The direct beam is linearly polarized with $P_p = 0.99$. Using the phase retarder, the degree of circular polarization is set such that $P_c > 0.9$. All measurement were performed at room temperature ($\sim 300\text{ K}$). The circular dichroism is usually characterized by an asymmetry that is defined as the ratio of the difference between the intensities I^+ and I^- and their sum, $A = (I^+ - I^-)/(I^+ + I^-)$, where I^+ corresponds to σ^+ ($e_x + i \cdot e_y$) and I^- to σ^- ($e_x - i \cdot e_y$) type helicity. Here, $e_{x,y}$ are the x and y components of the complex electric field vector describing circularly polarized photons propagating along the z axis. It is difficult, however, to establish a standard procedure for background subtraction. Moreover, small noise in the numerator of A can produce strongly divergent values when the denominator goes to zero after background subtraction. For this reason, the effects of the magnetic dichroism are simply shown as difference spectra $\Delta I = I^+ - I^-$.

4. Results and discussion

In the following, the magnetic circular dichroism in the photoelectron spectra of the $2p$ core level of Co and Fe will be presented and discussed. The spectra were taken from exchange biased thin CoFe and Co_2FeAl films, two materials that are widely used in spintronic devices. Firstly, results from the angular integrated mode will be reported to explain the basic effect. In the second part, details of the angular resolved measurements are presented. Finally, angular integrated magnetic dichroism in emission from the valence band will be presented.

4.1. Angular integrated magnetic dichroism.

As starting point, the regular – that is angular integrated, polarization dependent – photoemission spectra of the exchange-biased CoFe film were measured using the *transmission mode* of the spectrometer. The results are in well agreement to those reported earlier for similar systems [14]. As shown in Figure 3, the $2p$ core level spectra of Co (left panel) and Fe (right panel) exhibit a pronounced difference when taken with photons of opposite helicity for a fixed direction of magnetization. The pure difference $\Delta I = I^+ - I^-$ shown in Figure 3 contains all characteristic features of the magnetic circular dichroism.

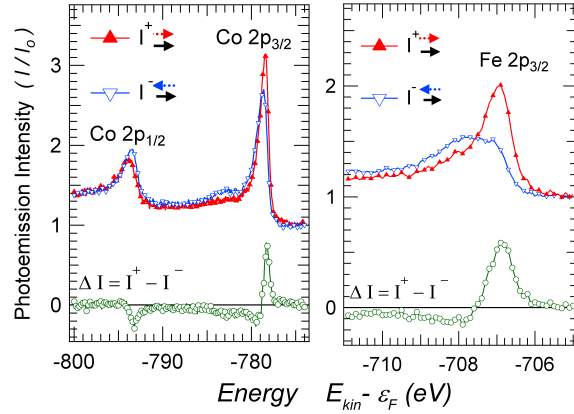


Figure 3: (Color online) Polarization-dependent photoelectron spectra of the Co $2p$ (left panel) and Fe $2p_{3/2}$ (right panel) core level emission from 10 nm-thick CoFe film on top of the MnIr exchange-biasing layer. I_0 represents the background intensity anteceding the lower energy tail. Dotted and solid arrows indicated the x-ray helicity and sample magnetization respectively. The difference spectra are represented by the open circles.

As one can see from Figure 3a, the spin-orbit splitting of the Co $2p$ states is clearly resolved. The dichroism changes its sign across the Co $2p$ spectrum in the sequence: $+ - - +$ when going from $p_{3/2}$ to $p_{1/2}$. This appears to be characteristic of a Zeemann-type m_j sub-level ordering as a consequence of the signs of the state multipoles ρ_{10} given in Table 1. The details of the MCDAD reveal, however, that the situation is more complicated. There are clear hints on multiplett splittings seen in the spectra. Close below the Co $p_{3/2}$ excitation, a low intense satellite is seen that exhibits clearly a dichroic signal. The asymmetry of this satellite is clearly higher (note the low intensity above background) compared to that at the maximum of the

Co $p_{3/2}$ intensity. Also, the dichroism in the Fe $2p$ spectrum does not vanish in the region between the spinorbit doublet, what complicates the analysis in terms of an asymmetry. It is a clear indicator for multiplet states that spread over the hole Fe $2p$ spectrum. The splitting of the Fe $2p_{3/2}$ is clearly more pronounced compared to Co $2p_{3/2}$. The details of the splitting and the dichroism have been discussed more detailed already in Reference [14].

4.2. Angular resolved magnetic dichroism.

In the next step, the angular distribution of the magnetic circular dichroism was investigated. In the previous experiments [14], the angular resolution was about $\pm 5^\circ$ and the electron detection was performed for normal emission only. Here, details of the magnetic dichroism will be studied over a 60° range of angles with a resolution of about 0.2° to 2° .

Figure 4 shows the $2p$ core level spectra of Co and Fe taken from the exchange biased Co_2FeAl film. The spectra were measured in the *angular mode*, which takes advantage of the wide-angle condenser lens system allowing the electrons to be collected over emission angles from -33° to $+33^\circ$ around normal emission. At the spectrometer, each channel of the detector covers an angle slice of 0.167° width. In general, measurements of the angular distribution of the photoelectrons using hard X-ray source and phase-retarder are very time consuming. The electron flux impinging each angular channel of the detector is very small resulting in a low accumulation rate and poor statistics compared to angular integrated spectra taken with the same integration time. For practical purposes, the spectra must be integrated over several channels to be analyzed.

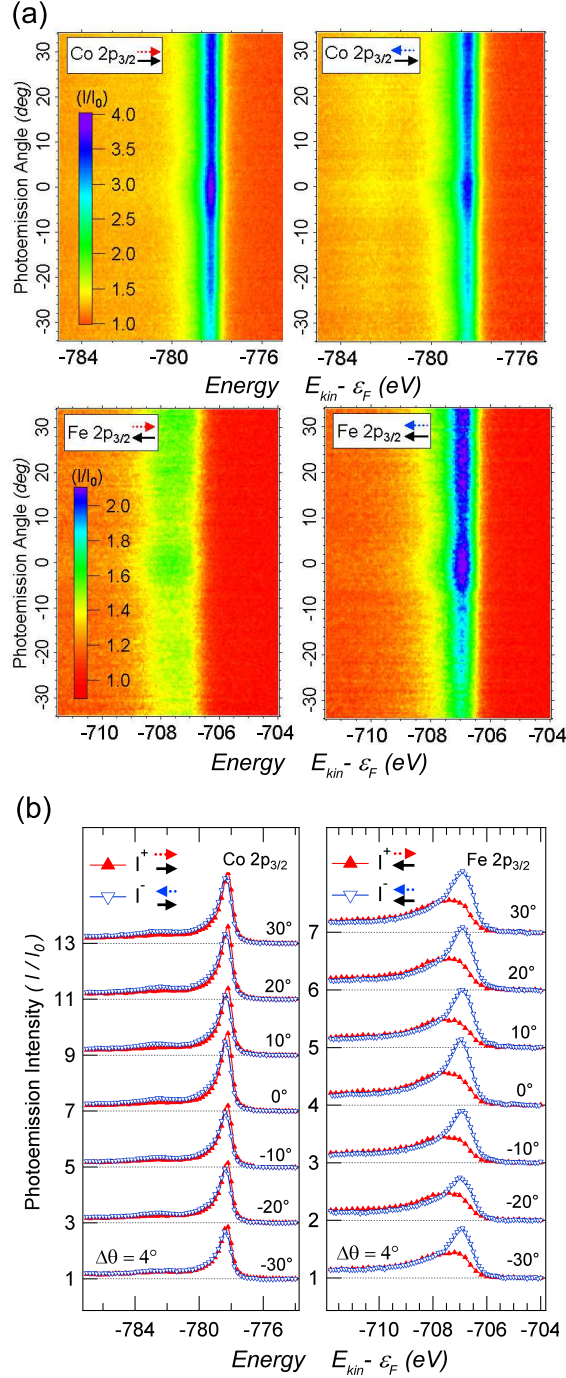


Figure 4: (Color online) Angular distribution of polarization-dependent photoelectron spectra of the Co and Fe $2p_{3/2}$ core level emission from 10 nm thick Co_2FeAl film on top of an MnIr exchange-biasing layer. I_0 represents the background intensity anteceding the lower energy tail. Dotted and solid arrows indicated the x-ray helicity and sample magnetization respectively. The bottom panel shows the EDC for both peaks and polarizations. Curves of different photoemission angles are integrated with a slice of 4° and are vertically offset from the zero value for clarity.

The energy distribution curves (EDC) are shown in the bottom panel of Figure 4. The spectra are summed up over slices of $\pm 2^\circ$ (12 channels) about the photoemission direction indicated by the label. No striking differences are noticed in spectral shape collected at different emission angles, but a strong dependence on the photon polarization is noticed in both, Co and Fe, $2p_{3/2}$ peaks. In comparison with the CoFe spectra (see Figure 3a), the Co $2p_{3/2}$ has a shift to lower binding energies and exhibits a smaller dichroism. The Fe $2p$ peaks in Co_2FeAl are similar to those measured from CoFe (see Figure 3b), where the spectral shapes for I^+ and I^- are exchanged due to the reversal of magnetization between the two samples.

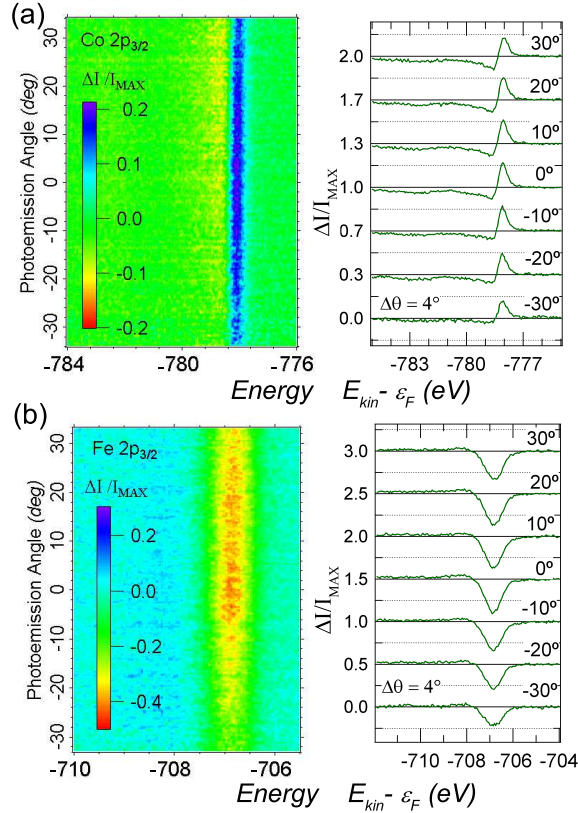


Figure 5: (Color online) Angular distribution of circular dichroism in the Co $2p_{3/2}$ (a) and Fe $2p_{3/2}$ (b) core-level photoemission from 10nm-thick Co_2FeAl film. ΔI is shown normalized by $I_{MAX}(\theta)$ which is the peak dispersion of the average photoemission (see text). Horizontal line-profiles are shown on right panels; curves for different photoemission angles are vertically offset from the zero value for clarity.

The angular dependence of the circular dichroism is shown in all details in Figure 5. The dichroism ΔI is normalized by $I_{MAX}(\theta)$, which represents the peak dispersion of the average spectra $I^{avg} = (I^+ - I^-)/2$. In this way, the angular dependence of the circular dichroism is free of structural contributions (e.g.: due to the forward scattering effect[27, 28]) and it results uniquely from the magnetic properties and symmetry of the electronic states. Note that, for both Fe and Co $2p_{3/2}$ peaks, there is an enhancement of dichroism about the normal direction. This is clearer seen from Figure 6. The \cos^2 function in Equation (1) leads to a maximum close to normal emission as is observed in the experiment. The small variation of the dichroism with angle of emission reveals that an atomic like description of the MCDAD as given above is sufficient to explain its most important features of the angular distribution. The complete energy dependence is, indeed, more complicated and is somehow hidden in the dynamical parameters C_{JkLN}^j of Equations (1) and (2). As mentioned above, these parameters include all possible multiplett and crystal field effects.

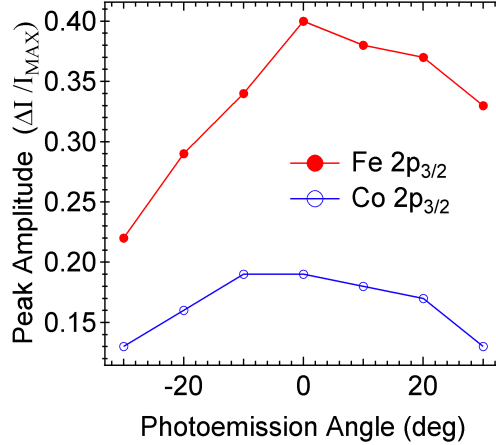


Figure 6: (Color online) Peak dispersion of $\Delta I/I_{MAX}(\theta)$ for the Co and Fe $2p_{3/2}$ states of the Co_2FeAl film.

4.3. Magnetic dichroism in valence band spectroscopy.

As already demonstrated in Reference [14], the magnetic dichroism is not only present in the photoelectron spectra of core level but also in valence band spectra. Different from excitation with UV photons [29, 30] and low kinetic energies, HAXPES does not reveal emission from single bands but

averages in k -space and is thus proportional to the density of states, indeed convoluted with the cross sections of the contributing states. It is not clear from beginning whether or not this allows to detect any magnetic circular dichroism, in particular when using an angular integrating mode.

Figure 7 shows the polarization dependence of the valence band spectra from the Co_2FeAl multilayer. It should be stressed that the valence band spectra have important contributions from the MnIr layer as well as from other underlying layers, nevertheless, a strong effect is still visible in the spectra near the Fermi energy when changing the helicity of the X-rays. Tentatively, this difference in the spectra is a consequence of a depletion of the occupied minority spin states close to the Fermi edge of the Co_2FeAl layer.

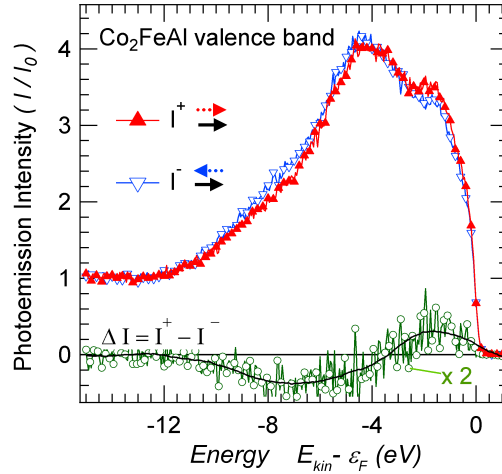


Figure 7: (Color online) Polarization-dependent photoelectron valence band spectra from 10nm-thick Co_2FeAl film on top of the MnIr exchange-biasing layer. Dotted and solid arrows indicated the X-ray helicity and sample magnetization respectively. The difference of the spectra taken with the opposite helicity of light is represented by open-circles and is shown enlarged by a factor of two.

Here the spectra are integrated in k -space over the initial states in the Brillouin zone as well as over a wide range ($\pm 33^\circ$) of emission angles. From the spectra and dichroism shown in Figure 7 it is obvious that magnetic circular dichroism is also observed in such integrated spectra. This demonstrates that magnetic dichroism can be observed even in the bulk sensitive spectroscopy of the total density of states at high kinetic energies (≈ 8 keV).

5. Summary and Conclusion

In summary, the feasibility to measure simultaneously the angular and energy distribution of the magnetic circular dichroism in photoelectron spectroscopy was demonstrated by use of a wide-angle lens setup installed at the HAXPES end-station of the beamline BL47XU at Spring-8. Bulk-sensitive HAXPES-MCDAD was used to image the electronic states and to study the magnetic response from buried layers. CoFe and Co₂FeAl ferromagnetic films grown on MnIr exchange-biased magnetic layers buried beneath MgO layers were analyzed. A strong dichroism was observed not only for core level but also in the valence band spectra of Co₂FeAl.

Recently, first spin resolved HAXPES experiments were reported [31, 32]. The much higher intensities (by three orders of magnitude) in spin integrated spectra makes HAXPES-MCDAD attractive for the studies of magnetic bulk materials and buried thin films in material science. HAXPES-MCDAD is particularly still the method of choice in valence band spectroscopy with low cross sections at high kinetic energies where the intensities are still too low for spin-resolved methods also with large angles of acceptance at the spectrometer.

Overall, the high bulk sensitivity of angular resolved HAXPES combined with circularly polarized photons will have a major impact on the study of the magnetic phenomena of deeply buried magnetic materials. It will allow an element-specific study of the magnetism of buried layers and make feasible the investigation of the properties of magnetic layers not only at the surface but also at buried interfaces.

Acknowledgments

The authors thank E. Ikenaga (Spring-8) for help with the experiments. D. E. thanks the group of G. Reiss (University of Bielefeld) for help with the sample production. Financial support by *Deutsche Forschungsgemeinschaft DFG* and the Strategic International Cooperative Program of the *Japan Science and Technology Agency JST* (DFG-JST) (Project P 1.3-A of research unit FOR 1464: *ASPIMATT*) is gratefully acknowledged. The HAXPES experiment was performed at BL47XU of SPring-8 with approval of JASRI (Proposal No. 2012A0043).

References

References

- [1] I. Lindau, P. Pianetta, S. Doniach, W. E. Spicer, *Nature* 250.
- [2] K. Kobayashi, M. Yabashi, Y. Takata, T. Tokushima, S. Shin, K. Tamasaku, D. Miwa, T. Ishikawa, H. Nohira, T. Hattori, Y. Sugita, O. N. A. Sakai, S. Zaima, *Appl. Phys. Lett.* 83 (2003) 1005.
- [3] S. Suga, A. Sekiyama, *Eur. Phys. J. Special Topics* 169 (2009) 227.
- [4] G. H. Fecher, B. Balke, A. Gloskowskii, S. Ouardi, C. Felser, T. Ishikawa, M. Yamamoto, Y. Yamashita, H. Yoshikawa, S. Ueda, K. Kobayashi, *Appl. Phys. Lett.* 92 (2008) 193513.
- [5] X. Kozina, S. Ouardi, B. Balke, G. Stryganyuk, G. H. Fecher, C. Felser, S. Ikeda, H. Ohno, E. Ikenaga, *Appl. Phys. Lett.* 96 (2010) 072105.
- [6] S. Ueda, H. Tanaka, J. Takaobushi, E. Ikenaga, J.-J. Kim, M. Kobata, T. Kawai, H. Osawa, N. Kawamura, M. Suzuki, K. Kobayashi, *Appl. Phys. Exp.* 1 (2008) 077003.
- [7] S. Ouardi, G. H. Fecher, X. Kozina, G. Stryganyuk, B. Balke, C. Felser, E. Ikenaga, T. Sugiyama, N. Kawamura, M. Suzuki, K. Kobayashi, *Phys. Rev. Lett.* 107 (2011) 036402.
- [8] L. Baumgarten, C. M. Schneider, H. Petersen, S. F, J. Kirschner, *Phys. Rev. Lett.* 65 (1990) 492.
- [9] D. Venus, *Phys. Rev. B* 48 (1993) 6144.
- [10] M. Getzlaff, C. Ostertag, G. H. Fecher, N. A. Cherepkov, G. Schönhense, *Phys. Rev. Lett.* 73 (1994) 3030.
- [11] N. A. Cherepkov, V. V. Kuznetsov, V. A. Verbitskii, *J. Phys. B: At. Mol. Opt. Phys.* 28 (1995) 1221–1239.
- [12] G. van der Laan, B. T. Thole, *Phys. Rev. B* 52 (1995) 15355.
- [13] F. U. Hillebrecht, C. Roth, H. B. Rose, W. G. Park, E. Kisker, N. A. Cherepkov, *Phys. Rev. B* 53 (1996) 12182.

- [14] X. Kozina, G. H. Fecher, G. Stryganyuk, S. Ouardi, B. Balke, C. Felser, G. Schönhense, E. Ikenaga, T. Sugiyama, N. Kawamura, M. Suzuki, T. Taira, T. Uemura, M. Yamamoto, H. Sukegawa, W. Wang, K. Inomata, K. Kobayashi, Phys. Rev. B 84 (2011) 054449.
- [15] H. Matsuda, H. Daimon, Japan Patent: PCT/jp2004/016602 Japan 208926 (2004).
- [16] H. Matsuda, H. Daimon, M. Kato, M. Kudo, Phys. Rev. E 71 (2005) 066503.
- [17] G. H. Fecher, V. V. Kuznetsov, N. A. Cherepkov, G. Schönhense, J. Electron Spectrosc. Relat. Phenom. 122 (2002) 157.
- [18] K. Blum, Density Matrix Theory and Application, Plenum, New York, 1981.
- [19] B. T. Thole, G. v. d. Laan, Phys. Rev. Lett. 67 (1991) 3306.
- [20] B. T. Thole, G. van der Laan, Phys. Rev. B 44 (1991) 12424.
- [21] B. T. Thole, G. v. d. Laan, Phys. Rev. B 50 (1994) 11474.
- [22] B. T. Thole, G. van der Laan, Phys. Rev. B 49 (1994) 9613.
- [23] G. H. Fecher, J. Elect. Spectros. Rel. Phenom. 114-116 (2001) 1165.
- [24] T. Marukame, T. Ishikawa, S. Hakamata, K.-i. Matsuda, T. Uemura, , M. Yamamoto, Appl. Phys. Lett. 90 (2007) 012508.
- [25] K. Kobayashi, Nucl. Instr. Meth. Phys. Res. A 601 (2009) 32 – 47.
- [26] M. Suzuki, N. Kawamura, M. Mizukami, A. Urata, H. Maruyama, S. Goto, T. Ishikawa, Jpn. J. Appl. Phys. 37 (1998) L1488.
- [27] H. C. Poon, S. Y. Tong, Phys. Rev. B 30 (1984) 6211.
- [28] J. W. F. Egelhoff, I. Jacob, J. M. Rudd, J. F. Cochran, B. Heinrich, J. Vac. Sci. Technol. A 8 (3) (1990) 1582.
- [29] C. M. Schneider, M. S. Hammond, P. Schuster, A. Cebollada, R. Miranda, J. Kirschner, Phys. Rev. B 44 (1991) 12066.

- [30] W. Kuch, C. M. Schneider, Rep. Prog. Phys. 64 (2001) 147.
- [31] A. Gloskovskii, G. Stryganyuk, G. H. Fecher, C. Felser, S. Thiess, H. Schulz-Ritter, W. Drube, G. Berner, M. Sing, R. Claessen, M. Yamamoto, J. Electron Spectrosc. Relat. Phenom. 185 (2012) 47.
- [32] G. Stryganyuk, X. Kozina, G. H. Fecher, S. Ouardi, S. Chadov, C. Felser, G. Schönhense, P. Lushchik, A. Oelsner, P. Bernhard, E. Ikenaga, T. Sugiyama, H. Sukegawa, Z. Wen, K. Inomata, K. Kobayashi, Jpn. J. Appl. Phys. 51 (2012) 016602.